Pressure-induced structural phase transition of paracrystalline silicon

Murat Durandurdu and D. A. Drabold

Department of Physics and Astronomy, Ohio University, Athens, Ohio 45701-2979

We report on the pressure-induced phase transition in a model of paracrystalline silicon (amorphous silicon with a crystalline grain) using an *ab initio* constant pressure simulation technique. The paracrystalline model transforms into a high-density amorphous phase at 16 GPa with a discontinuous volume change of ~24%. The transformation of the crystalline grain begins at the boundary and proceeds into the core. We also study the pressure-induced crystallization of the network using the Gibbs free-energy calculation and find a transition from the paracrystalline silicon to β-Sn at 3−4 GPa. The electronic nature of the pressure-induced semiconductor-metal transition is discussed.

I. INTRODUCTION

The application of pressure to solids leads to a diverse collection of interesting phenomena. The most dramatic may be pressure-induced insulator-metal phase transitions. The pressure-induced phase transitions in crystalline silicon (c-Si) have been studied extensively. The diamond structure of c-Si transforms into a metallic β-Sn phase around 9.5−12 GPa.[1−3] Under further compression, c-Si undergoes a structural transformation from the β-Sn to an *Imma* structure at 13 GPa.[4] The *Imma* phase transforms into the simple hexagonal (sh) structure near 16 GPa.[2−4] The hexagonal closed packed (hcp) structure is observed at 42 GPa.[2,3] In addition, a phase Si(VI) between sh and hcp is obtained at 39 GPa.[2] Recently the structure of Si(VI) was identified as orthorhombic with 16 atoms per unit cell and space group symmetry *Cmca*.[5] On release of pressure, c-Si does not transform back to the diamond structure. Instead, a metastable $BC8$ phase is recovered on slow pressure release from the β-Sn,[6] while two tetragonal phases are obtained from very rapid pressure release.[7] The *expanded* phase of silicon, clathrate Si_{136} with a wide gap of ~2 eV, transforms to a β-Sn structure at 8 GPa.[8]

The behavior of amorphous silicon (a-Si), porous silicon (p-Si), and nanocrystalline silicon under pressure, however, is very different from that of diamond and clathrate. Nanocrystalline silicon transformed directly to a sh structure at 22 GPa.[9] Upon pressure release, an *Imma*, β-Sn, and finally an amorphous phase was recovered. In p-Si, a diamond to β-Sn transformation was reported.[10] However, Deb *et al.* showed pressure-induced amorphization of diamond silicon at 15−16 GPa in a p-Si sample.[11] That is, the crystalline portion of the sample appears to transform to a high-density amorphous phase upon compression.

For a-Si, contradictory high-pressure data has been reported. Amorphous samples obtained using pressure-induced amorphization exhibited a sharp phase transition to β-Sn at 8 GPa on compression.[12] We note that samples formed by this method contain crystalline grains and have some different physical properties compared to amorphous thin films.[13] The crystallization of a-Si, however, was not seen in other investigations, and instead a high-density disordered phase was obtained.[14−16]

Fluctuation electron microscopy[17] investigations have shown that as-deposited amorphous silicon thin films exhibit significant medium-range order, which is interpreted as indicating the presence of small-crystalline grains (<30 Å) embedded in a disordered matrix.[18−20] The grains have crystalline topology, with some distortions induced by the grain boundaries. Since the grains are dilute and deformed, they are difficult to separate from the amorphous "background" using diffraction experiments. Nevertheless, the grains contribute significant medium-range order to the amorphous thin films, which is detectable by fluctuation electron microscopy. Such materials have been designated *paracrystalline*.[19] In this paper, we study the pressure-induced phase transition in a 400-atom model of paracrystalline silicon (*para*-Si) including a single-crystalline grain, using an *ab initio* constant pressure-relaxation simulation. We find that the model undergoes a first-order phase transition to a high-density amorphous phase at 16 GPa. On the other hand, the Gibbs free-energy calculation predicts a structural transformation from the *para*-Si model to a β-Sn structure at 3−4 GPa. The discontinuous metallization of the network is in agreement with experimental studies of amorphous thin films[14,15] and computer simulation of a continuous random network model of a-Si.[16] It is also found that the localized electronic states at zero pressure become extended with the application of pressure.

II. METHODOLOGY

The simulations reported here are carried out on a 400-atom model of *para*-Si. The *para*-Si model is generated using a generalized version of the bond-switching method of Wooten, Winer, and Weaire.[21] The model has one grain consisting of 44 atoms. It has a structure factor and electronic density of states essentially identical to continuous random network models of a-Si.[22] Compared to a 4000-atom model with four crystalline grains of roughly the same size (100 atoms), the 400-atom model does not reproduce the fluctuation microscopy signal, which indicates that the medium-range order is not realistic. Nevertheless, the simulation does faithfully model a crystalline grain embedded in an amorphous matrix. At zero pressure, the 400-atom model is relaxed with a local orbital first-principles quantum molecular-
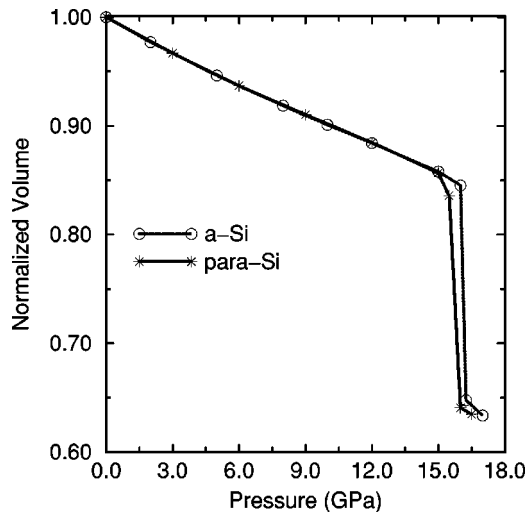
FIG. 1. The normalized volume of *para*-Si and *a*-Si as a function of pressure.

dynamics method of Sankey and Niklewski.[23] The method employs the density-functional theory within the local-density approximation using the Harris functional with hard norm-conserving pseudopotentials. This Hamiltonian was successfully applied in *c*-Si including high-pressure phases,[23] expanded volume phases of silicon ("zeolites without oxygen"),[24] *a*-Si.[25,26] The combination of this *ab initio* technique with the Parrinello and Rahman method[27] was employed to study a first order amorphous to amorphous phase change in Si (Ref. 16) and Ge,[28] a continuous amorphous to amorphous phase transformation in GeSe$_2$,[29] ZB→*Cmcm*→*Imm*2 transitions in GaAs,[30] a diamond to simple hexagonal phase transition in Si,[16] and a diamond to β-Sn phase change in Ge.[28] Pressure is increased in an increment of 3 GPa up to 15 GPa, after which an increment of 0.5 GPa is carried out in order to accurately estimate the transition pressure. For each value of the applied pressure, we fully relax the system according to the criterion that the maximum force is smaller than 0.01 eV/Å. The optimization is performed with the conjugate-gradient technique. We use Γ-point sampling for the supercell's Brillouin-zone integration, which is reasonable for a 400-atom model. A fictitious cell mass of 11×10^3 amu was found to be suitable for this simulation.

III. RESULTS AND DISCUSSIONS

A. Structural properties

The pressure volume curve of the *para*-Si model is depicted in Fig. 1. The volume changes smoothly up to 15.5 GPa, and at which point it drops $\sim 2.5\%$. At 16 GPa, an abrupt decline of the volume is seen, indicating a first-order pressure-induced phase transition. The volume drops about 24%, which is close to the value of ~ 21–23% reported in the diamond to β-Sn transformation of *c*-Si.[31,32] The discontinuous metallization of the model is in agreement with the experimental result on conductivity of the amorphous thin films[14,15] and the previous simulation of *a*-Si.[16] Crystallization of the model is not observed, and instead a transition
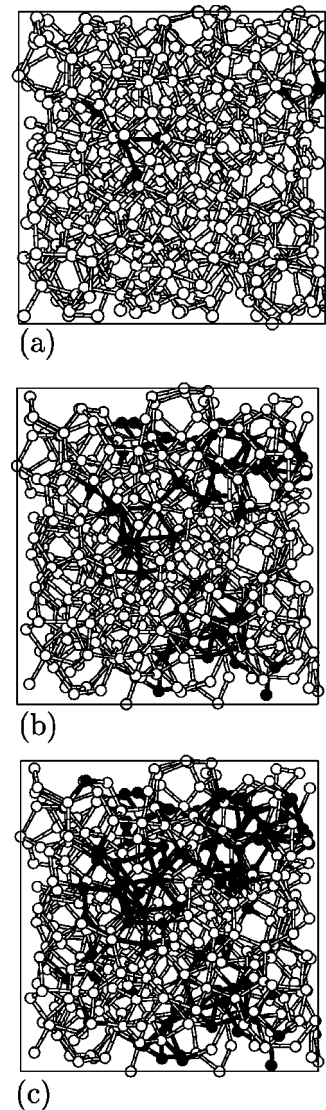
FIG. 2. Nucleation centers define in the model at (a) 15 GPa, (b) 15.5 GPa, and (c) 16 GPa (an intermediate step). Black atoms have coordination >4.

from diamond to a high-density amorphous phase is seen, which was recently reported in a *p*-Si sample with an average crystalline size of ~ 50 Å.[11]

To show the evolution of high-density nucleation centers, we visualize the model at three different pressures in Fig. 2. The white atoms represent fourfold coordinated atoms whereas the black ones correspond to higher coordinated atoms (>4). At 15 GPa, the nucleation begins in the vicinity of defects with large bond angle deviations, which enable distortions leading to a more close packed topology. At 15.5 GPa and an intermediate step at 16 GPa, the size of the higher coordinated clusters grows. This result suggests that the transition in the *para*-Si model is not homogeneous.

Dramatic structural changes are seen at the boundary of the grain after the normalized volume reaches a value of 0.8. At this volume, $\sim 20\%$ of the disordered matrix transforms to a highly coordinated geometry, but the crystalline grain still persists in the network. Although the size of crystalline
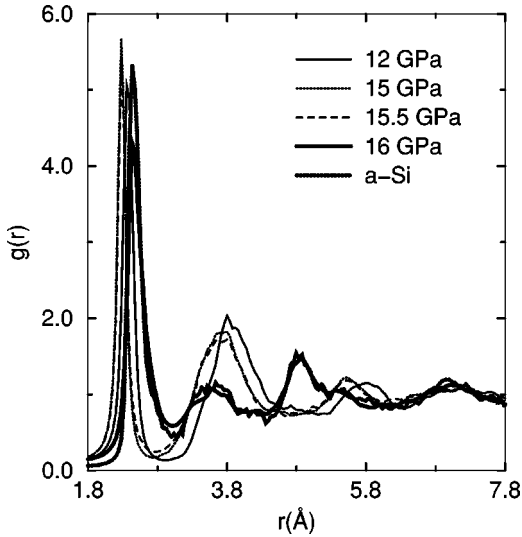
FIG. 3. The real-space pair distribution function $g(r)$ of the *para*-Si model under pressure. $g(r)$ of the *a*-Si model is also given at the transition pressure (16.25 GPa).

grain in the model is small, we find that the transformation of the grain begins at the interface and gradually proceeds into the core.

The real-space pair distribution function $g(r)$ is given in Fig. 3. The peak positions shift to shorter distances, indicating tighter packing of the network, with pressure up to 16 GPa. The intensity of the peaks changes slightly until the transition pressure, at which a huge coordination change is observed. At the transition pressure, the intensity of the first peak decreases abruptly with a broadened distribution, and its position moves to a larger distance, reflecting a much higher ($\approx$ eight- to ninefold) coordination. The intensity of the second peak exhibits a sharp decrease, and its position shifts toward a shorter distance.

The bond angle distribution function of the model is shown in Fig. 4. The model retains ideal (fourfold) coordi-
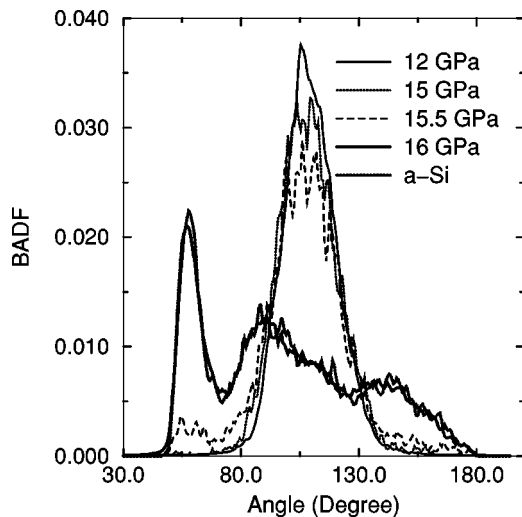
FIG. 4. The bond angle distribution function (BADF) of the *para*-Si model, and the *a*-Si model at transition pressure.

TABLE I. Structural properties of the *para*-Si model under pressure: average bond length (ABL), average bond angle (ABA), width of bond angle distribution (WBAD), and average coordination number (ACN).

Pressure (GPa)	0	12	15	15.5	16
ABL (Å)	2.38	2.308	2.29	2.31	2.55
ABA	109.22°	108.9°	108.69°	106.90°	98.07°
WBAD	10.47°	11.58°	12.90°	18.67°	32.97°
ACN	4.000	4.000	4.015	4.200	8.975

nation up to 12 GPa shows a smooth distribution with a single peak centered at the tetrahedral angle. Above this pressure, the distribution is broadened with a significant decrease in the intensity. At 15.5 GPa, a peak appears near 60° in the distribution due to the higher coordinated topology. At the transition, the function is rather broad with important peaks around 60°, 90°, and 150°. The peak at 60° is a clear indication of a close-packed geometry with metallic bonding.

The structural properties of the *para*-Si geometry under the application of pressure are presented in Table I. The compression up to 15 GPa causes the narrowing of tetrahedral angles, and shortened bond lengths with no increase in the coordination. At the transition, the average coordination from the first minimum of $g(r)$ within a critical cutoff radius $r_c = 3.02$ Å is found to be 8.9 and quite sensitive to choice of the cutoff radius. The average bond length changes from 2.31 to 2.55 Å, and the average bond angle drops to 98.07°, which is intermediate between the tetrahedral and octahedral values of 109.5° and 90°, respectively.

B. Gibbs free energy calculation

In order to study crystallization of the model, we compute the volume dependence of Gibbs free energy. Diamond, β-Sn, and *para*-Si are optimized for several volumes and fit to the Birch-Murnaghan equation of state. We report the minimum structural energy per atom E_{min} and corresponding atomic volume V_{min} for each structure in Table II. For diamond and β-Sn structure, the relative total-energy difference per atom ($\Delta E_{min} = E_{min}^{\beta-Sn} - E_{min}^{diamond}$) and the ratio of the equilibrium volume ($V_{min}^r = V_{min}^{\beta-Sn}/V_{min}^{diamond}$) are found to be 0.289 eV/atom and 0.74, respectively. These values are comparable to 0.27 eV/atom and 0.77 reported in accurate self-consistent calculations.[31]

TABLE II. The minimum energies E_{min}, the relative energy difference $\Delta E = E^i - E^{diamond}$, the corresponding minimum volume per atom V_{min}, and its ratio $V_{min}^r = V_{min}^i/V_{min}^{diamond}$, where i is diamond, β-Sn, and *para*-Si phase.

Structure	Diamond	β-Sn	*para*-Si
E_{min} (eV/atom)	−108.006	−107.717	−107.826
ΔE_{min} (eV/atom)	0	0.289	0.183
V_{min} (Å³/atom)	20.76	15.42	21.20
V_{min}^r	1.0	0.74	1.013
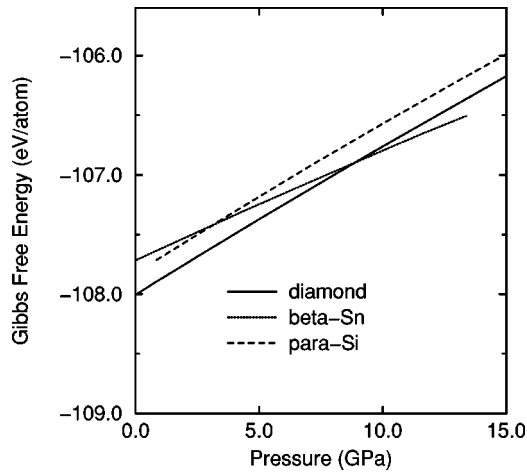
FIG. 5. Gibbs free-energy curve of c-Si, β-Sn, and $para$-Si.

The calculated Gibbs free energies ($G = E_{tot} + PV$) at zero temperature for diamond, β-Sn, and the $para$-Si structure are shown in Fig. 5. The transition pressure between diamond and β-Sn phase is found to be 9 GPa, which is consistent with the result of 9.5–15.4 GPa reported in previous experiment and theoretical studies.[32] The transition volume of diamond V_t(diamond) and β-Sn V_t(β-Sn) is 0.924 and 0.684, respectively. V_t(diamond) value is in good agreement with experiment and theoretical results of 0.89–0.928 whereas the transition volume of β-Sn is less than 0.70–0.719.[32]

The Gibbs free-energy curve of the $para$-Si network and β-Sn crosses about 3–4 GPa, indicating a first-order phase
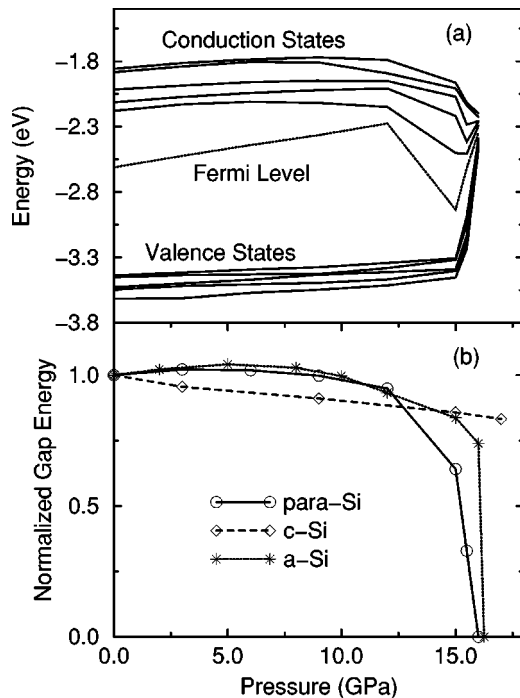
FIG. 6. (a) Pressure dependence of energies of some tail states and the Fermi level. (b) The normalized optical gap for $para$-Si, c-Si, and a-Si as a function of pressure.
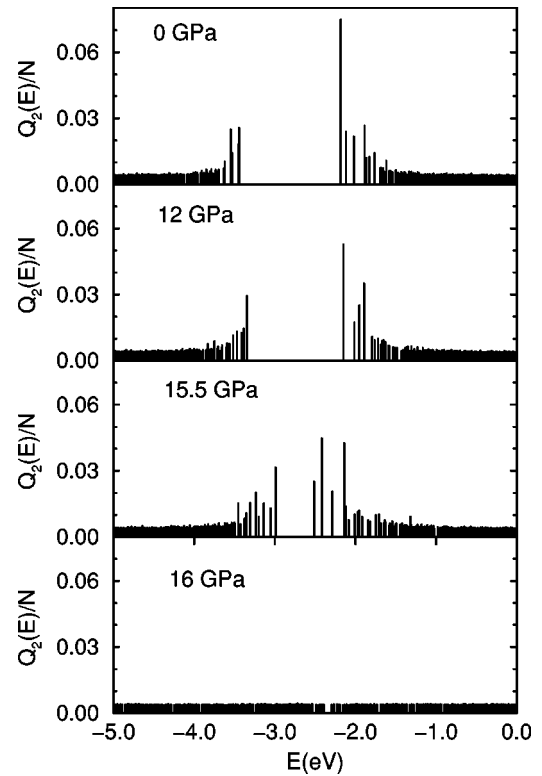
FIG. 7. The localized states near the band gap. Q_2 is the inverse participation ratio, measuring spatial localization of the state. Note the delocalization at 16 GPa, clearly reflecting a metallic state.

transition. The critical pressure of this transition is less than that of the diamond to β-Sn transformation. The transition obtained between the $para$-Si model and β-Sn agrees with the experimental study of a-Si under pressure but, the predicted crystallization pressure (3–4 GPa) is much less than 8 GPa, which is probably due to the relative energy difference between the $para$-Si structure and c-Si ($\Delta E_{min} = E_{min}^{para} - E_{min}^{diamond} = 0.183$ eV). This value is higher than an experimental result 0.0977 eV for a-Si, as extrapolated to 0 K from the measurement at 960 K using the specific heat listed in that work.[33] When the slope of the common tangent line is considered in energy volume curve, a network with a small energy difference at the same minimum volume yields an increase of the slope and so the transition pressure.

One expects that there is no easy pathway between $para$-Si and β-Sn structure, and the crystallization requires bond breaking and a large displacement of some atoms in contrast to the diamond to β-Sn transition. The displacement of atoms is hindered at low temperatures and needs more thermal activation. Thus the crystallization of $para$-Si is kinetically inhibited in the simulation.

C. Electronic structure

The application of silicon depends strongly on the nature of the electron states near the Fermi level. The pressure dependence of a few tail states and the Fermi level are given in Fig. 6. The valence tail states tend to move gradually toward the center of the band gap up to 15.5 GPa, and after this

pressure the shift of the states becomes more dramatic. The conduction tail states shift into higher energies at low pressures. With further increase of the pressure, the states begins to move to lower energies. When the higher coordination is encountered in the network at 15 GPa, the states move abruptly to the middle of the band gap. The Fermi level exhibits a smooth increase up to 12 GPa. Above this pressure, it shifts to a lower energy. When the topology has higher coordination, the conduction tail states and the Fermi level reveal a complex behavior.

In amorphous tetrahedral materials, the optical gap increases with pressure (0–1 GPa).[34,35] The pressure coefficient of the fundamental absorption in a-Si is positive, $+0.25$ meV/kbar,[34] whereas it is negative in c-Si, -1.5 meV/kbar,[34] and in a-Si:H, -1 meV/kbar.[37,36] Figure 6 shows the pressure dependence of the optical gap of c-Si and a-Si and $para$-Si. The optical gap of c-Si decreases smoothly with the application of pressure, and the pressure derivative of the gap is found to be -1.73 meV/kbar in the pressure range 0–17 GPa, which is consistent with the experimental result of -1.5 meV/kbar.[34] However, the behavior of the $para$-Si and a-Si model under pressure is different from that of c-Si: It increases initially, reaches a maximum, and then decreases under pressure. Above 12 GPa, the gap of the $para$-Si declines because of the increase in the coordination. In the pressure range 0–6 GPa, we find that the pressure derivative of the band gap in the $para$-Si model is $+0.39$ meV/kbar, which is comparable to $+0.25$ meV/kbar value of amorphous silicon.[34]

In order to study the pressure dependence of the localization of electron states, we define the Mulliken charge,[38] $Q(n,E)$, for atom n associated with the eigenvalue E. This charge can then be used as a measure of the localization of a given state $Q_2(E) = N\Sigma_{n=1}^{N} Q(n,E)^2$, where N is the number of atoms in a supercell. For a uniformly extended state,

$Q_2(E)$ is 1, while it is N for a state perfectly localized on a single atom. The localization of the electron states near the band gap is depicted in Fig. 7. As expected, the states near the band gap are quite localized at zero pressure, and the localization of these states decreases gradually, indicating pressure-induced delocalization of the states, similarly to that found in the a-Si (Ref. 16) and the a-GeSe$_2$ model.[29] At the transition pressure, the tail states are abruptly delocalized as seen in the a-Si networks.[16]

IV. CONCLUSIONS

We have studied the pressure-induced phase transition in a 400-atom model of $para$-Si using an ab $initio$ constant pressure relaxation technique. The model undergoes a first-order phase transition into an amorphous metallic phase. The transition is inhomogenous and begins in the vicinity of defects. The embedded crystalline (diamond) grain transforms to a high disordered topology, which is consistent with the study of p-Si under pressure. The transition of the gain begins at the boundary and proceeds into the bulk. In order to reveal the size effects of the crystalline grains, it is worth repeating these types of calculations using large models with a different size of grains. A Gibbs free-energy calculation predicts the pressure-induced crystallization of the $para$-Si network. We find that the small increase of the coordination dramatically changes the electronic structure of the model.

[1] M. C. Gupta and A. L. Ruoff, J. Appl. Phys. **51**, 1072 (1980).

[2] H. Olijnyk, S. K. Sikka, and W. B. Holzapfel, Phys. Lett. **103A**, 137 (1987).

[3] J. Z. Hu, L. D. Merkle, C. S. Menoni, and I. L. Spain, Phys. Rev. B **34**, 4679 (1986); J. Z. Hu and I. L. Spain, Solid State Commun. **51**, 263 (1984).

[4] M. I. McMahon and R. J. Nelmes, Phys. Rev. B **47**, 8337 (1993); M. I. McMahon, R. J. Nelmes, N. G. Wright, and D. R. Allan, *ibid.* **50**, 739 (1994).

[5] M. Hanfland, U. Schwarz, K. Syassen, and K. Takemura, Phys. Rev. Lett. **82**, 1197 (1999).

[6] S. Kasper and M. S. Richards, Acta Crystallogr. **17**, 752 (1964).

[7] Y. X. Zhao, F. Buehler, J. R. Sites, and I. L. Spain, Solid State Commun. **59**, 679 (1986).

[8] G. Ramachadran, P. F. McMillan, S. K. Deb, M. Somayazulu, J. Gryko, Jianjun Dong, and O. F. Sankey, J. Phys.: Condens. Matter **12**, 4013 (2000).

[9] S. H. Tolbert, A. B. Herhold, L. E. Brus, and A. P. Alivisatos, Phys. Rev. Lett. **76**, 4384 (1996).

[10] J. Zeman, M. Zigone, G. L. J. A. Rikken, and G. Martinez, J. Phys. Chem. Solids **56**, 655 (1995).

[11] S. K. Deb, M. Wilding, M. Somayazulu, and P. F. McMillan, Nature (London) **414**, 528 (2001).

[12] V. Domnich and Y. Gogotsi, Rev. Advan. Mat. Science **3**, 1 (2002); V. Domnich, Y. Gogotsi, and M. Trenary, in Mater. Res. Soc. Symp. Proc. No. 649 (Materials Research Society, Pittsburgh, 2001).

[13] V. V. Brazhkin, A. G. Lyapin, V. A. Goncharova, O. V. Stal'gorova, and S. V. Popova, Phys. Rev. B **56**, 990 (1997).

[14] O. Shimomura, S. Minomura, N. Sakai, K. Asaumi, K. Tamura, J. Fukushima, and H. Endo, Philos. Mag. **29**, 547 (1974).

[15] S. Minomura, *High Pressure and Low-Temperature Physics* (Plenum, New York, 1978), p. 483.

[16] M. Durandurdu and D. A. Drabold, Phys. Rev. B **64**, 014101 (2001).

[17] P. M. Voyles, J. M. Gibson, and M. M. J. Treacy, J. Electron Microsc. **49**, 259 (2000).

[18] M. M. J. Treacy and J. M. Gibson, Acta Crystallogr., Sect. A: Found. Crystallogr. **A52**, 212 (1996).

[19] M. M. J. Treacy, J. M. Gibson, and P. J. Keblinski, J. Non-Cryst.

Solids **231**, 99 (1998).

[20] M. M. J. Treacy, P. M. Voyles, and J. M. Gibson, J. Non-Cryst. Solids **266**, 150 (2000).

[21] G. T. Barkema and N. Mousseau, Phys. Rev. B **62**, 4985 (2000).

[22] S. M. Nakhmanson, P. M. Voyles, N. Mousseau, G. T. Barkema, and D. A. Drabold, Phys. Rev. B **63**, 235207 (2001).

[23] O. F. Sankey and D. J. Niklewski, Phys. Rev. B **40**, 3979 (1989).

[24] A. A. Demkov, W. Windl, and O. F. Sankey, Phys. Rev. B **53**, 11 288 (1996).

[25] P. A. Fedders, D. A. Drabold, and S. Nakhmanson, Phys. Rev. B **58**, 15 624 (1998).

[26] M. Durandurdu, D. A. Drabold, and N. Mousseau, Phys. Rev. B **62**, 15 307 (2000).

[27] M. Parrinello and A. Rahman, Phys. Rev. Lett. **45**, 1196 (1980); S. Nose and M. L. Klein, Mol. Phys. **50**, 1055 (1983).

[28] M. Durandurdu and D. A. Drabold, Phys. Rev. B **66**, 041201 (2002).

[29] M. Durandurdu and D. A. Drabold, Phys. Rev. B **65**, 104208 (2002).

[30] M. Durandurdu and D. A. Drabold, Phys. Rev. B **66**, 045209 (2002).

[31] M. T. Yin and M. L. Cohen, Phys. Rev. B **26**, 5668 (1982).

[32] F. Zandiehnadem and W. Y. Ching, Phys. Rev. B **41**, 12 162 (1990).

[33] E. P. Donovan, F. Spaepen, D. Turnbull, J. M. Poate, and D. C. Jacobson, J. Appl. Phys. **57**, 2782 (1985).

[34] G. A. N. Connell and W. Paul, J. Non-Cryst. Solids **8−10**, 215 (1972).

[35] T. Tanaka, J. Non-Cryst. Solids **90**, 363 (1987).

[36] S. Minomura, J. Phys. (Paris), Colloq. **42**, C4-181 (1981); in *Semiconductors and Semimetals*, edited by J. I. Pankove (Academic, Orlando, 1984), Vol. 21A, p. 273.

[37] T. Tanaka, Phys. Rev. B **39**, 3258 (1989).

[38] A. Szabo and N. S. Ostlund, *Modern Quantum Chemistry* (Dover, New York, 1996).